Engineering Fracture Mechanics 184 (2017) 88–100

Contents lists available at ScienceDirect

Engineering Fracture Mechanics

journal homepage: www.elsevier.com/locate/engfracmech

Reaction products from electrode fracture and Coulomb explosions in batteries

A. Widom [a], Y. Srivastava [a,*], J. Swain [a], Georges de Montmollin [b], L. Rosselli [b]

[a] Physics Department, Northeastern University, Boston, MA, USA
[b] Lenr-Cities Suisse Sàrl, Rue Charles Knapp 29, CH-2000 Neuchâtel CH, Switzerland

ARTICLE INFO

Article history:
Received 5 July 2017
Received in revised form 14 August 2017
Accepted 18 August 2017
Available online 24 August 2017

ABSTRACT

We re-examine published theories that predict large acceleration of electrons for materials under great stress and that successfully describe neutron and other particle production in natural phenomena as well as in laboratory experiments. A fracture mechanics analysis obeying Griffith's law allows us to deduce the critical micro-crack size and elastic stresses essential for estimating the electric fields; boosts in the Lorentz factor of the electrons and towards the expected frequency spectrum of electro-magnetic radiation in micro-cavities. They are also applied here to study the energetics behind shredding and fracture of a cathode in a battery under substantial dc voltages ($\geqslant$ 400 V). We show quantitatively that the electric fields generated and the subsequent acceleration of electrons and ions at the tip of a shredding cathode can be comparable to that in fracturing rocks and other geophysical processes. Some experimental evidence showing production of new elements is presented. We also reconsider previous theory and experiments about Coulomb explosions and establish easy and proper protocols for the Coulomb explosions of alkali metals in our quest for establishing processes-beyond purely chemical-discovered in other electrolytes.

1. Introduction

While studies about fracture of materials under stress are legion that are described in standard texts [1,2], only recently have they been theoretically studied [3–8] with an eye towards neutron and other particle production when brittle materials undergo fracture and shredding under extreme stress. Experimentally, radioactive emissions from geophysical fracturing of rocks in the earth's crust just prior to large earthquakes have been observed [9,10]. Neutrons have also been observed from bolts of lightning [11] and from thunderstorms [12]. An excellent review of the experimental situation about neutron and other particle production from fracture, both in nature and in the laboratory, can be found in a book [13] and more recently in [14], where the observed fracto-emissions are successfully described through applications of the electro-weak and electro-strong theory [6–8].

Another experimentally well established path, actively followed over the past two decades, leading to neutron and other particle creation (called LENR, low energy nuclear reactions) is through Coulomb explosions [15–20]. In the pioneering experiments [15,16], electrons were removed from a beam of deuterium atoms resulting in clusters of positively charged nuclei, deuterons. Once the charge density of a cluster exceeded a critical value (discussed later), the cluster exploded and the deuterons flying out acquired quite large kinetic energies [$\geqslant$ several *keV*'s]. When two such deuterons (from

* Corresponding author.
E-mail address: yogendra.srivastava@gmail.com (Y. Srivastava).

http://dx.doi.org/10.1016/j.engfracmech.2017.08.030
0013-7944/

different clusters) "met", they could easily overcome their mutual Coulomb repulsion and cause a nuclear reaction. The by now legendary *dd* fusion reaction observed through Coulomb explosions

$$d + d \rightarrow {}^{3}\mathrm{He} + n, \tag{1}$$

has since then been confirmed by several groups and other reactions studied. The process has been refined and sufficiently under control, so much so that even the angular distribution of the reaction products has been measured [17].

But deuterons are not mandatory since, Coulomb explosions can also be arranged for highly reactive alkali atoms, such as lithium, sodium and potassium, as well as nickel, all materials we have experimented with, and successfully exploded. As we shall describe in the following in some detail, the observed lithium Coulomb explosions are strikingly similar to lithium battery explosions, raising therefore the exciting possibility that the "usual" lithium battery explosions are not entirely chemical. We conjecture that there is indeed a nuclear component. We shall briefly consider the necessary conditions for LENR to occur in Coulomb explosions and describe our experimental work in progress towards establishing the same.

In Section 2, we provide a brief theoretical background that includes a mechanical fracture analysis essential to an understanding of the new phenomena and motivations behind the particular set of experiments performed and described in the present paper. The first set of our experiments and their analysis described here concerns the fracture and shredding of electrodes in an electrolytic cell; i.e. in a battery. We discuss some simple experiments carried out by electrolysis fracture and shredding in both copper and tungsten cathode wires in Section 3. During the fracturing process, a bright plasma glow may be observed on the tip of the cathode, however the plasma is by no means a requirement for the production of new materials in the cell [21]. Many nuclear reactions in the plasma glow mode have been observed by Mizuno [22–25] and by Cirillo [26] employing scanning electron microscope (SEM) and energy dispersive spectroscopy (EDX) techniques probing those product atoms left on the cathode.

An alternative route to the pioneering plasma cell experiments referred to above is presented in the present paper. We focus on a particular aspect, the energetics and dynamics of shredding and fracture of electrodes through *electro-weak* and *electro-strong* theories alluded to above and relate it to our experimental set up and observations.

The final nuclear reaction products may often be described by reactions of the form

$$\begin{aligned} &e^- + p \rightarrow n + \nu_e, \\ &[\text{electron capture}] \\ &n + {}^{A}X_Z \rightarrow {}^{A+1}X_Z, \\ &[\text{neutron absorption or halo nuclei}] \\ &{}^{A+1}X_Z \rightarrow {}^{A+1}X_{Z+1} + e^- + \bar{\nu}_e, \\ &[\text{Fermi beta decay process}] \end{aligned} \tag{2}$$

together with other similar *electro-weak* LENR chains. We shall discuss *electro-strong* LENR processes later.

In Section 3 we discuss the reactions associated with tungsten and copper cathode probes carrying electrons through the electrolyte to a stainless steel anode. The voltage across the chemical cell was 400 V when employing a copper as cathode and a bi-sodium carbonate or a lithium hydroxide electrolyte carrying a current of about 5 A, depending on the state of disrepair of the cathode. The fractured shredding of the copper wire cathode was made manifest by the powdered grains that formed an almost opaque colloidal suspension within the electrolyte. After a few days, the colloidal grains drifted to the bottom of a storage bowl leaving the electrolyte clear. Evidence of a new element was found on the partially shredded copper cathode wires. A similar experiment starting with distilled water at the same high 400 V source, yielded a small current of about 4 m-A, depending on the state of disrepair of the tungsten cathode. At such small currents there is no visible plasma near the tungsten tip. Nevertheless, high voltage shredding of the tungsten occurred over a long time scale of ten hours.

2. Theoretical background & motivation behind the experiments

In this section, we shall first briefly summarize our previously published theoretical analyses concerning both *electro-weak* and *electro-strong* methods of inducing LENR that were anchored on an underlying well established mechanical fracture analysis. These theoretical results provided us the motivation for performing the particular set of LENR experiments through fracture and shredding in electrolysis (both with and without the generation of visible plasma) as well as through Coulomb explosions caused in nickel and alkali metals, lithium in particular.

2.1. Theoretical background

The electro-weak induction of LENR of interest for the present paper proceeds through (i) an electric field acceleration of electrons and protons (or, ions) arising from fracture of materials, followed by (ii) the Fermi weak interactions described in Eq. (2). The acceleration of said electrons is essential for producing a neutron (of mass M_n) since $[(M_n - M_p - m_e)c^2 \approx 0.78\ \mathrm{MeV}]$ of energy has to be provided to the $(e^- p)$ system (of mass m_e & M_p respectively) to overcome the mass-energy gap so that the reaction

$$W_{electric} + e^- + p \rightarrow n + \nu_e, \tag{3}$$

can proceed. One method proposed is to electrically activate plasmon oscillations of a frequency (Ω) with an electric field of magnitude ($\mathcal{E}$) on the surface of metallic hydrides that possess a high density of electrons and protons. Neutron production would be triggered when the electron mass-energy as quantified by its Lorentz boost factor γ exceeds a "threshold value" quantified below:

$$V_{eff} = \left(\frac{c\mathcal{E}}{\Omega}\right) = \sqrt{(\gamma^2-1)}\left(\frac{mc^2}{e}\right) = \sqrt{(\gamma^2-1)}(0.511\ \text{MV}) \geqslant 1.23\ \text{MV};\ \gamma > 2.6. \tag{4}$$

Such very low energy neutrons born in micron or smaller scale surface regions have a very small mean free path [~ 10 Å] to escape as free particles since their nuclear absorption cross-section with other nuclei is quite high. Thus they are expected to yield a long list of nuclear transmutations through their absorption in the host nuclei.

An important role is played here by the *halo* nuclei, wherein a very low energy neutron is loosely attached to some nucleus A to form a much larger (nA) halo nucleus, that may exist for a considerable period of time. The probability of forming such halo nuclei is quite high since the neutron absorption cross-section rises as $(1/v)$ for a small neutron velocity v. Further nuclear physics description of halo nuclei can be found in [27].

Let us consider an example of *electro-weak* lithium cycle when low energy neutrons are available. Successive absorption of neutrons can produce ${}^4_2\text{He}$:

$$\begin{aligned} {}^6_3\text{Li} + n &\rightarrow {}^7_3\text{Li} \\ {}^7_3\text{Li} + n &\rightarrow {}^8_3\text{Li} \\ {}^8_3\text{Li} &\rightarrow {}^8_4\text{Be} + e^- + \bar{\nu}_e \\ {}^8_4\text{Be} &\rightarrow {}^4_2\text{He} + {}^4_2\text{He}. \end{aligned} \tag{5}$$

There is a substantial amount of heat produced through the above reaction

$$Q\{{}^6_3\text{Li} + 2n \rightarrow 2\ {}^4_2\text{He} + e^- + \bar{\nu}_e\} \approx 26.9\ \text{MeV}. \tag{6}$$

On the other hand, the produced ${}^4_2\text{He}$, if it does not escape, can reproduce ${}^6_3\text{Li}$ nuclei:

$$\begin{aligned} {}^4_2\text{He} + n &\rightarrow {}^5_2\text{He} \\ {}^5_2\text{He} + n &\rightarrow {}^6_2\text{He} \\ {}^6_2\text{He} &\rightarrow {}^6_3\text{Li} + e^- + \bar{\nu}_e \end{aligned} \tag{7}$$

The heat produced through Eq. (7) is

$$Q\{{}^4_2\text{He} + 2n \rightarrow {}^6_3\text{Li} + e^- + \bar{\nu}_e\} \approx 2.59\ \text{MeV}. \tag{8}$$

Thus, taken together, the complete cycle can produce a reasonably large amount of heat. Of course, other channels are possible that not only produce ${}^4_2\text{He}$ but also ${}^3_2\text{He}$.

Estimates of neutron production rates from *electro-weak* reactions have been made in [4,5,26]. These range from $(10^{12}$–$10^{14})$ neutrons/(cm^2 s), depending upon the process under consideration.

We here mention a channel of possible relevance later (see, Section 3.1), when we discuss new products produced in electrolysis with lithium hydroxide as an electrolyte. In Eq. (5), a highly unstable isotope of beryllium [${}^8_4\text{Be}$] is produced that decays resonantly to two helium-4 nuclei. On the other hand, if it could absorb a further neutron, it would produce the (only) stable isotope ${}^9_4\text{Be}$:

$${}^8_4\text{Be} + n \rightarrow {}^9_4\text{Be}. \tag{9}$$

The decay mode ${}^8_4\text{Be}$ into two helium nuclei as in Eq. (5), plays an important role in stellar nuclear dynamics and is thus well studied, while the neutron absorption mode to form stable ${}^9_4\text{Be}$ is not, for the simple reason that there is not an ample supply of neutrons in the previous context. However, both channels proceed through strong (nuclear) interactions. The half-life of ${}^8_4\text{Be}$ is about 67 ns. We can estimate the rate of formation of ${}^9_4\text{Be}$ as follows.

$$Rate = \rho v \sigma_{absorption} \approx \rho v \sigma_{total} = \rho v \left[\frac{4\pi\hbar}{Mv}\right] \Im m F(0), \tag{10}$$

where ρ is the nuclear density, M is the neutron mass and $F(0)$ is the forward elastic amplitude. If we insert the nominal values: $\Im m F(0) \approx 1$ fermi and standard nuclear density $\rho = 10^{23}/\text{cm}^3$, then we find for a rate of approximately 10^8/s. This would yield a formation time of about 10 ns, a bit smaller but of the same order of magnitude as the decay time. Within the uncertainties inherent in the computation, we can conclude is that our suggested mechanism can -under favourable conditions of enough neutrons- indeed lead to the production of stable beryllium from lithium.

We now briefly review the relevant parts of electro-strong induction of LENR discussed in [6,8] that are of interest to the present paper. Consider for example, the fracture of Fe_3O_4 magnetite rocks; i.e., magnetic semi-conductor loadstones. The

fracture process accelerates electrons, which in turn produce electromagnetic radiation. Such radiation can cause photo-disintegration of the iron nucleus through giant dipole resonances (GDR) [28]:

$$\gamma + {}^{56}\mathrm{Fe} \rightarrow {}^{56}\mathrm{Fe}^{*} \rightarrow (\text{fission products}). \tag{11}$$

The total (GDR) cross-section for absorbing a photon has the peak value

$$\sigma_o = [4\pi Z\alpha]\frac{\hbar}{M\Gamma}, \tag{12}$$

where $Z = 26$ is the nuclear electric charge in this case, $\alpha \approx 1/137.036$ is the fine-structure constant, M is the proton mass and Γ is the total fission decay rate of the compound nucleus. Typically, the GDR energies are in the range (10–20) MeV for heavy nuclei and (15–25) MeV for light nuclei.

If in accordance with the liquid drop model, the compound nucleus ${}^{56}\mathrm{Fe}^{*}$ decays preferentially into two equal excited Aluminum droplets

$${}^{56}\mathrm{Fe}^{*} \rightarrow 2\,{}^{28}\mathrm{Al}^{*}, \tag{13}$$

and if each droplet beta-decays into

$${}^{28}\mathrm{Al}^{*} \rightarrow {}^{28}\mathrm{Si} + e^{-} + \bar{\nu}_e, \tag{14}$$

the final decay channel reads

$$\gamma + {}^{56}\mathrm{Fe} \rightarrow 2[{}^{28}\mathrm{Si} + e^{-} + \bar{\nu}_e];\ (\text{two Si channel}). \tag{15}$$

Clearly, a host of other channels are also possible and many such have been experimentally observed [13,14].

Both electro-weak and electro-strong schemes require large acceleration of electrons. In the following Section 2.2, we review the tools from fracture mechanics necessary for a quantitative study of particle accelerations and other core aspects of the new phenomena.

2.2. Fracture mechanics and new phenomena

We briefly review the mechanics of fracturing materials from established engineering point of view and how it gets related to various new phenomena observed in a laboratory or in geophysical situations (e.g., generation of large electric and magnetic fields; acceleration of electrons and ions; micro wave radiation, earthquake lights, neutron production, etc.)-some of them-being discussed in the present paper. Such connections have been developed at length in two previous publications [6,8].

Piezo-electric materials (PEM) are well known to produce electric fields when under stress [29]. Hence, generation of large electric fields through PEM were considered in [6]. Since fracturing granite (that contains substantial amounts of quartz, a natural PEM) has been shown to produce neutrons both in the laboratory [14] as well as in earthquakes [13], crucial steps in the theoretical analysis of particle production presented in [6] involved schematically:

$$\begin{aligned}
&\sigma(\text{Stress}) \ \Rightarrow\ \mathcal{E}(\text{Electric Field})\\
&[\textit{through PEM}]\\
&\sigma_c(\text{Critical Stress}) \ \Longleftrightarrow\ a(\text{microcrack length})\\
&[\textit{through Griffith's law}]\\
&\mathcal{E} \ \Rightarrow\ \gamma(\text{Lorentz boost})\\
&[\textit{through Lorentz Force}]\\
&\text{Large } \gamma \Rightarrow\ \text{particle production}\\
&[\textit{through electroweak } \& \textit{ electrostrong}]
\end{aligned} \tag{16}$$

Shown in Fig. 1 is a crystal under stress σ inducing a micro-crack of width $2a$ and length $L \gg a$. The energy U_b required to create a micro-crack of width $2b$ and length L is given by [30]

$$u(b) = \frac{U_b}{L} = 4\gamma_s b - \pi\left[\frac{(1-\nu^2)\sigma^2}{Y}\right]b^2, \tag{17}$$

wherein γ_s is the surface tension of the micro-crack interface, ν is the Poisson ratio and, Y is the Young's modulus of the material.

The maximum of the elastic micro-crack energy per unit length $[max_{b>0}u(b)]$ represents the energy barrier to the creation of a micro-crack

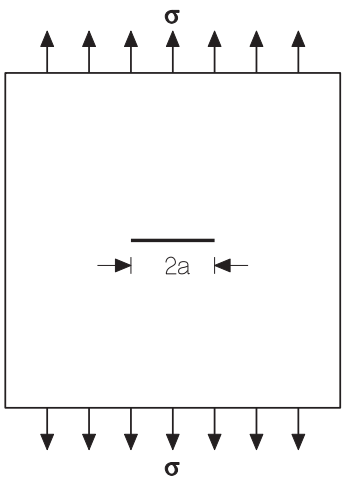

Fig. 1. A micro-crack is formed in a solid under stress σ. The width of the micro-crack is $2a$ and the length L (into the paper) has $L \gg a$. The half width a is the critical length size for forming the micro-crack as discussed in Eq. (18).

$$
\begin{aligned}
&u = max_{b>0} u(b); \ \text{for } b = a \\
&a = \frac{2\gamma_s}{\pi}\left[\frac{Y}{(1-\nu^2)\sigma_F^2}\right]; \\
&u = 2\gamma_s a = \frac{4\gamma_s^2}{\pi}\left[\frac{Y}{(1-\nu^2)\sigma_F^2}\right]
\end{aligned}
\tag{18}
$$

The level of stress σ_F that nucleates a micro-crack is given by the well-known Griffith result [31], as discussed in [30]

$$
\sigma_F = \sqrt{\frac{2\gamma_s Y}{\pi(1-\nu^2)a}}. \tag{19}
$$

If σ_{bond} denotes the elastic stress required to break the chemical bonds over the area of the micro-crack, given by

$$
\sigma_{bond} = \frac{2Y}{\pi(1-\nu^2)}, \tag{20}
$$

then the tensile strength σ_F is related to σ_{bond} via the equation

$$
\sigma_F = \sqrt{\frac{\sigma_{bond}\gamma_s}{a}}; \ \Rightarrow \ \sigma_F \ll \sigma_{bond}, \tag{21}
$$

for brittle fracture.

Numerical analysis of experiments on brittle fracture of granite (containing a large amount of fused quartz) has been made in [6] leading to the following estimates:

$$
\begin{aligned}
&\gamma_s \sim \ 10^2\left[\frac{\text{erg}}{\text{cm}^2}\right] \sim \ 10^{-1}\left[\frac{\text{J}}{\text{m}^2}\right]; \\
&\sigma_F \sim \ 10^9\left[\frac{\text{erg}}{\text{cm}^3}\right] \sim \ 10^8\left[\frac{\text{J}}{\text{m}^3}\right]; \\
&\sigma_{bond} \sim \ 10^{12}\left[\frac{\text{erg}}{\text{cm}^3}\right] \sim \ 10^{11}\left[\frac{\text{J}}{\text{m}^3}\right]; \\
&a \sim \ 1\ \mu\text{m}; \\
&L \sim \ 20\ \mu\text{m}.
\end{aligned}
\tag{22}
$$

It is satisfactory that *a posteriori* (i) $\sigma_F \ll \sigma_{bond}$ obeying Griffith's law; and (ii) $a \ll L$.

The numerics obtained from the mechanical analysis and the size of micro-wave cavities were then used to estimate electro-magnetic quantities as (i) the required electric field $\mathcal{E}$ for fracture and (ii) the micro-wave frequency Ω, that are essential for the estimation of the EM acceleration of electrons [that is, the Lorentz factor γ] through Eq. (4) to determine whether electro-weak processes can be induced and thus neutrons produced:

$$\mathcal{E} \sim 1.12 \times 10^5 \text{ G} = 3.36 \times [10^7 \ \frac{\text{V}}{\text{cm}}];$$
$$\Omega \sim \left[\frac{10^{10}}{\text{s}}\right]$$
$$\gamma \sim 100. \tag{23}$$

The above numbers far exceed the threshold value and thus lead to a robust rate for neutron production. It was further observed [6] that if the fracture occurs through a hydraulic fracture process, then the neutron production rate would be further enhanced due to a higher concentration of water on the micro-fracture surface areas.

Anticipating our electrolysis experiments discussed in the next section, it is worthy of note that the theoretically predicted generation of micro-waves has been verified. In Supplementary material to the present paper that can be found on the web site [32], some examples of the frequency spectrum of radiation produced through electrolysis are exhibited.

Under conditions of magnetic rock crushing, the magnetization changes also give rise in the micro-cracks to microwave radiation. Microwaves in turn give rise to accelerated electrons with energies $\gamma(mc^2)$. The average electric field ($\mathcal{E}$), the microwave frequency (Ω) and the Lorentz factor γ, for this case, have been estimated to be [8]

$$\mathcal{E} \approx 3.3 \times 10^5 \text{ G} \sim 10^{10} [\text{V/m}];$$
$$\Omega \sim 10^{10}/\text{s};$$
$$\gamma(mc^2) \sim 150 \text{ MeV}. \tag{24}$$

Such energetic electrons can easily cause photo-disintegration of iron nuclei through electro-strong processes and thus produce a host of fission products.

2.3. Past Coulomb explosion experiments

As discussed earlier in the Introduction, there is yet another method to induce LENR, through Coulomb nuclear explosions.

In early experiments, exploding molecular clusters of deuterium atoms were produced. First, a weak laser pulse hit the cluster internally ionizing the atoms within the cluster. It was then followed by a strong laser pulse photo-ejecting a large number of electrons completely out of the molecular cluster. This left the cluster with a large positive charge ($Q = Ne$) in a sphere of small radius R. Clusters with large Q in a small R explode. Ejected deuterons from different clusters then collided with sufficient kinetic energy to overcome the Coulomb barrier and led to clean observation of fusion events. Such experiments have now been repeated in several laboratories around the world and results bear out their theoretical analysis (such as the size of the clusters, the rate and the channels of fusion reactions).

Let us estimate what (order of) magnitudes for the fields are required for a Coulomb explosion. Let V, $\mathcal{E}$ and P denote respectively the voltage, electric field and the stress on the system of charges.

$$V = \frac{Q}{R} = \frac{Ne}{R};$$
$$\mathcal{E} = \frac{Q}{R^2} = \frac{Ne}{R^2};$$
$$P = \frac{\mathcal{E}^2}{8\pi} = \frac{N^2 e^2}{8\pi R^4}. \tag{25}$$

The *tensile strength* of a material P_c is defined as the maximum allowed stress before the material disintegrates.

$$\mathcal{E}_c = \sqrt{8\pi P_c};$$
$$\textit{for } \mathcal{E} < \mathcal{E}_c, \ \textit{material} \Rightarrow \textit{stable};$$
$$\textit{for } \mathcal{E} > \mathcal{E}_c, \ \textit{material} \Rightarrow \textit{unstable}. \tag{26}$$

Typical explosion fields are of the order of

$$\mathcal{E}_c \sim \ [10^{10} \div 10^{11}] \text{ V/m}. \tag{27}$$

We have seen above in Eq. (11) that similar fields were produced in magnetite fracture causing electro-strong LENR. There is a physical reason for this similarity: all electronic bonds are severed under such strong electric fields.

We can deduce a "hot" disintegration temperature T_c for Coulomb explosion devices, using Eqs. 25 and 26:

$$eV_c = k_B T_c \sim \left(\frac{R}{100\text{Å}}\right) \text{KeV}; \ T_c \sim \ 10^7 \text{ K}, \tag{28}$$

of the order of the temperature near the core of the Sun.

Through the collision between two deuterons from different clusters, in Refs. [15–17], the production of neutrons has been observed via the reaction:

$$d + d \rightarrow {}^{3}He(0.82\ \mathrm{MeV}) + n(2.45\ \mathrm{MeV}), \tag{29}$$

the peak of their signal showing up at the expected characteristic neutron energy of (2.45 ± 0.2) MeV.

The success achieved with deuteron fusion, led to a series of experiments using other molecular clusters [18,19] through which detailed dynamical mechanisms for the explosions could be understood along with the structure of the molecules themselves. It has become an imaging tool as well; see for instance [20].

2.4. Motivation behind the experiments

The motivation behind the electrode fracture (and their shredding) experiments described here is to probe the electro-weak and electro-strong theory of LENR summarized in Section 2.1.

The motivation behind the lithium experiment is to first establish a necessary protocol for its Coulomb explosion without having a molecular cluster set up as in Section 2.3. This is in an effort to probe in the future whether there is a nuclear component (in addition to the chemical component) in the lithium battery explosions.

2.5. Energetics of electrolysis experiments

Let us estimate the relative input energy consumption between Mizuno-Cirillo cells employing plasma (that only lasted for several minutes) [Method (1)] & cells without plasma, the Dash-cell [Method (2)] that can last for several hours or even days.

Method 1: Here the numerics are as follows:

$$\begin{aligned} &V_{in} = \text{Input voltage } = 400\ \mathrm{V};\\ &I_s = \text{average steady current } = 5\ \mathrm{A};\\ &T_r = \text{running time } = 300\ \mathrm{s}.\\ &E^{I}_{in} = \text{Input energy} = V_{in} \times I_s \times T_r = 6 \times 10^5\ \mathrm{J} \end{aligned} \tag{30}$$

Method II: The numerics here are

$$\begin{aligned} &V_{in} = \text{Input voltage} = 400\ \mathrm{V};\\ &I_s = \text{average steady current } = 4 \times 10^{-3}\ \mathrm{A};\\ &T_r = \text{running time} = 10\ \mathrm{h} = 3.6 \times 10^4\ \mathrm{s}.\\ &E^{II}_{in} = \text{Input energy} = V_{in} \times I_s \times T_r = 5.76 \times 10^4\ \mathrm{J} \end{aligned} \tag{31}$$

Under the assumption (to be verified experimentally) that nuclear transmutations through both methods are of similar strength, clearly Method II, apart from being more stable, would also require an order of magnitude less input energy than for Method I and hence would appear preferable for further study and development.

In Section 3 *et sec.*, we shall describe the details of our experiments.

3. Copper and tungsten cathodes

A copper cathode and a stainless steel anode were lowered into a strong $(Na^+)_2CO_3^-$ electrolyte in water. An anode-cathode voltage of four hundred volts was applied yielding an anode current of approximately five amperes. Initially, the electrolyte was clear with some gas bubbles rising into the atmosphere at both the anode and cathode corresponding to the normal water electrolysis. Also, the copper cathode shred colloidal grains into the fluid. The colloidal electrolyte eventually turned cloudy with plasma still visible. The copper cathode was considerably shortened due to the shredding of particles that entered into the colloid. The colloidal electrolyte was later stored in a glass bowl for a few days. The colloidal particles sedimented at the bottom of the bowl.

3.1. Chemical states of a copper electrode

The "pure copper" blank electrode was analyzed for surface chemical contamination as shown in Fig. 2. Apart from small oxide concentrations and organic carbon deposits on the surface, the purity of the blank copper sample is shown to be of satisfactory quality.

An energy dispersive spectra was taken near the copper electrode tip *after* being treated by the plasma in a lithium hydroxide electrolyte. In Fig. 3 the region of the copper electrode that was analyzed is exhibited. The resulting energy dispersive spectra is exhibited in Fig. 4. Very worthy of note is an anomalously large peak labeled by the EDX machine as beryllium. Since the EDX spectra is almost always too small to be detected for lithium, boron and perhaps beryllium due

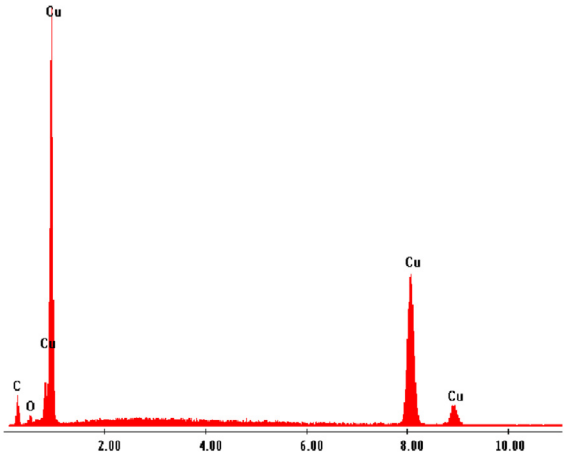

Fig. 2. An energy dispersive spectra (EDX) of our pure copper electrode wire before any electrolytic treatment or plasma. The wire surface contains some oxide and organic carbon impurities. But the spectra in the main is that of pure copper.

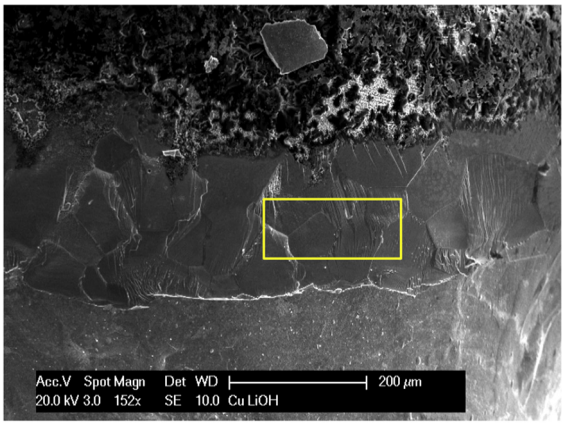

Fig. 3. A scanning electron microscope picture of a region near the tip of a copper cathode after being in part shredded by a plasma in lithium hydroxide. A region was selected for an energy dispersion analysis as shown.

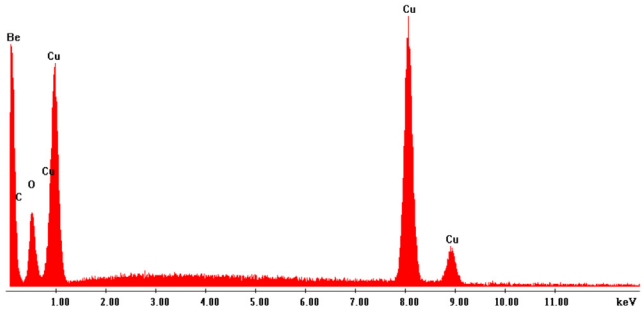

Fig. 4. An energy dispersive spectra of atoms in the region shown in Fig. 3. The vertical scale is arbitrary. Apart from the atoms observed in the pure blank electrode in Fig. 2, one finds an anomaly induced by the plasma in the form of a very large peak that the EDX machine labels as beryllium. Filtering this large new peak, one finds that what is really present is a mixture of boron and beryllium as would be expected for a nuclear lithium chain started from the lithium in the electrolyte plasma.

to the very low atomic numbers and since the line shape of the spectra was also somewhat anomalous, filtering was applied that revealed both boron and beryllium [35]. Since the plasma is white hot, we attribute the boron and beryllium mixture to be the product of a lithium cycle chain that had been predicted theoretically in previous work and appears in stellar nuclear

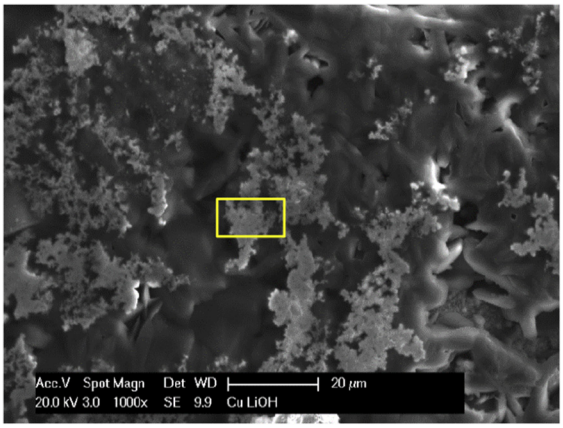

Fig. 5. A scanning electron microscope picture of a region near the tip of a copper cathode after being in part shredded by a plasma in a lithium hydroxide electrolyte. The spatial scale is smaller than that chosen in Fig. 3.

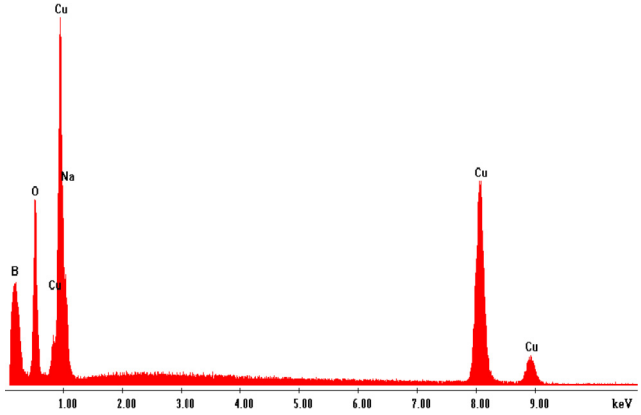

Fig. 6. The small grain structure has a peak labeled by the EDX machine as boron but which after filtering is shown to be a mixture of boron and beryllium. The new peak is due to sodium atoms within the grains. This is most easily explained by giant dipole resonant disintegration of the copper nuclei within the cathode surface.

physics work [4,33]. We have extended these previous theoretical results to understand and explain the presence of new observed elements in the present electrolysis via Eqs. (5), (9) and (10) *et sec.*

To examine the energy dispersive structure for a copper cathode in a LiOH electrolyte plasma on a smaller spatial scale, we chose a region as shown in Fig. 5. Here one detects grains on a small length scale of about ten microns which is perhaps a factor of ten smaller than in Fig. 3. The energy dispersive spectra on this smaller scale is shown in Fig. 6. The small length scale energy structure of the grains indicates one new element apart from the boron and beryllium nuclear transmutations. Within the grains there is a strong sodium peak in the EDX spectra. The sodium peak can be explained via the collective giant dipole resonant disintegration [6–8] of the copper nuclei in an electrode that is being shredded.

The Young's modulus of copper is $Y = 1.20 \times 10^{11}$ Pa. Thus, the electric field required to shred copper can be estimated from the analysis in (2.2) to be larger than $\mathcal{E} \geqslant 9 \times 10^{11}$ V/m. Near the tip of the electrode immersed in water, the field-over atomic distances-may be considerably larger.

On the other hand, the peak of giant dipole resonance (GDR) for copper is at a photon energy $E_\gamma \approx 17$ MeV with a width $\Gamma \approx 7$ MeV [34].

Thus, an *electro-strong* GDR disintegration of copper, leading to many final states, is perfectly feasible for a cavity frequency Ω of the order of 10^{10} Hz.

3.2. Chemical states of a tungsten electrode

An ordinary electrolysis was performed employing a pure tungsten cathode and a stainless steel anode in a distilled water electrolyte. A SEM-EDX picture of the blank tungsten rod is shown in Fig. 7. At a high voltage of about a half kilovolt, the very low conductivity of the electrolyte yielded a current of about five milli-amperes dependent on the state of disrepair of the

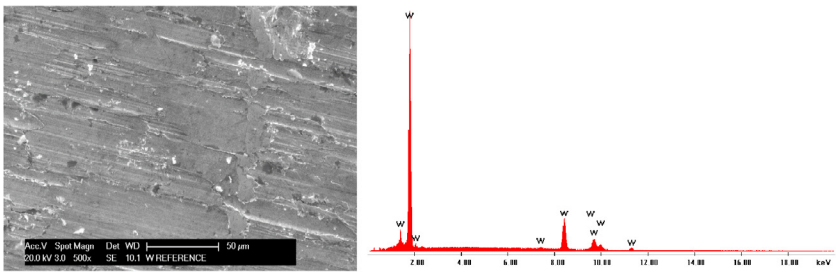

Fig. 7. The SEM picture of the blank tungsten rod before electrolysis is shown along with the EDX spectrum indicating that the blank was pure tungsten to a sufficient degree of accuracy.

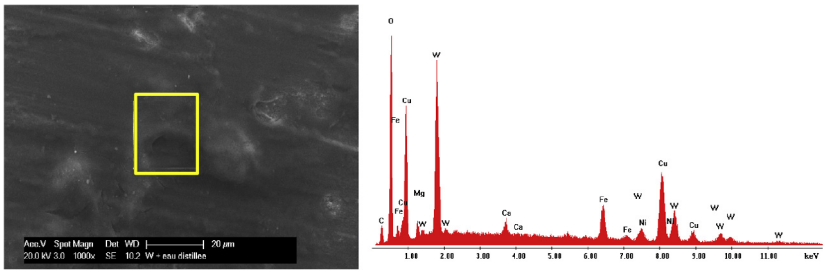

Fig. 8. SEM-EDX picture of a typical region of the tungsten electrode after ten hours of electrolysis starting from a distilled water electrolyte. A large variety of new chemical elements is present on the cathode due to the shredding of tungsten. The elements added to tungsten are copper, iron, calcium, magnesium and nickel. The amount of copper from nuclear transmutations is anomalously large.

cathode. The currents were much too low to produce an electrolyte plasma. Before the electrolyte turned yellow, at least in part due to tungsten oxides, the chemical cell was run for about ten hours. The resulting electrolyte plated out in part on the cathode and in part on the anode.

In spite of the lack of an electrolyte plasma, the chemical cell apparently produced a large variety of nuclear transmutations during the shredding process into electrolyte colloidal particles that, in part, floated on top of the fluid. The large variety of atoms detected on the tungsten cathode after ten hours of electrolysis depended in detail on which part of the cathode was observed. A typical picture is exhibited in Fig. 8. In Eq. (32) below are shown the atomic fractions of elements on the tungsten cathode therein *after* electrolysis for ten hours.

Element	Atomic %
Mg	6.35
Ca	3.45
Fe	12.42
Ni	6.65
Cu	49.07
W	22.05

(32)

The nuclear transmutations into copper are particularly striking. The copper is in fact visible to the naked eye as a golden-red granular deposit on the cathode in almost all regions near the tungsten cathode tip.

We can repeat the GDR calculations for tungsten as done earlier for copper. The Young's modulus of tungsten is $Y = 4.11 \times 10^{11}$ Pa. Thus, the electric field required to shred tungsten can again be estimated as in the previous case to be $\mathcal{E} \geqslant 3 \times 10^{11}$ V/m.

The peak of giant dipole resonance (GDR) for (the four stable isotopes of) tungsten is at a mean photon energy $E_\gamma \approx 13$ MeV with a width $\Gamma \approx 6$ MeV [34].

Once again, an *electro-strong* GDR disintegration of tungsten, leading to a plethora of final states, becomes feasible for a cavity frequency Ω of the order of 10^{10} Hz.

4. Lithium ion battery explosions

It is a well known feature of lithium ion batteries that from time to time they explode producing hot flames and pouring water over the flames very often merely increases the heat of the explosion. To study this phenomenon we needed a reliable way to produce lithium explosions in the laboratory.

Exploding melted droplets of alkali metals have been studied in some detail [36,37]. When liquid alkali metal droplets are dropped from a height of the order of a meter into water they at first lose their electrons, then they Coulomb explode. Through fast photography, in [36] a direct blue electron solvated in water profile was established along with a time interval for Coulomb explosions to develop-of about half a milli-second-after the droplets hit the water. They were also able to estimate the minimum charge separation to be 5 Å. It is interesting to observe that the electric field generated by a total charge Q at this distance is $6(Q/e) \times 10^9$ V/m. Thus, a modest value of separated charge Q, can bring us to the familiar value of critical electric fields that occur in all the examples of fracture and explosions discussed in the earlier sections of the present paper.

Let us note [for our own experiments to be described below] that when a pellet is dropped from the height of a meter, the velocity at impact is about 4.4 m/s. It was found in [37], that when the droplets were dropped from smaller heights, blue solvated electrons were still visible, but the system could be kept in the non-explosive regime.

In the following subsections, we shall describe two different protocols for obtaining Coulomb explosions.

4.1. Coulomb explosions with melt and water

We produced liquid lithium explosions by putting some lithium in a Pyrex glass dish and melted at least in large part the lithium. Then cool water was poured over the lithium melt and a lithium explosion ensued. In Fig. 9, the explosion is exhibited. There is the white hot plasma near where the lithium was, as well as a "balled lightning white hot plasma" that here jumped out of the glass bowl and fell onto the table top. Above the plasma is fire and smoke which can result if the lithium grains are not fully melted. For water poured over solid grains there is no white hot plasma but merely smoke given off by the lithium. The reader must be warned that the smoke can trigger a building alarm which may bring some attention to this experiment from local police and fire departments. However, the experimental explosions are simple and entirely reproducible preferably with a gas path to blow the smoke through a safety duct.

While the dynamics of the material left in the dish are left for future study, it is possible to estimate the average speed of the objects flying out of the dish as shown in Fig. 9. The initial average speed v_o can be estimated by comparison to the average vertical height $\langle H \rangle$ of the (vertically) flying out objects through $v_o = \sqrt{2g\langle H \rangle}$, where $g \approx 9.8$ m/s^2 is the acceleration due to gravity. Over many experimental trials, we found $\langle H \rangle \sim 1$ m and thus $\langle v_o \rangle \sim 4.4$ m/s, in satisfactory agreement with the velocity of the flying out objects $v_o = 4.4$ m/s, the "threshold" speed found in [36] when dropped from a height of exactly 1 m for ensuring Coulomb explosion. Thus, our results confirm that the phenomenon being discussed is indeed a Coulomb explosion. Of course, what remains inside the dish requires further careful analysis as mentioned earlier.

Provided the yet to be verified necessary conditions discussed in Section 4.3 are satisfied, the balled lightning plasmas discussed in this work should produce neutrons and thereby nuclear transmutations as does ordinary lightning [11].

4.2. Coulomb explosions through lasers

Here we describe another protocol for causing satisfactory Coulomb explosions of alkali metals (lithium, sodium and potassium) as well as that of nickel, through the energy supplied by an inexpensive fixed intensity (*not* requiring a femtosecond) laser and also without the need of a beam of atoms as required in [15,16].

The energy deposited by the [5×10^{17} W/cm^2] femtosecond laser employed in [15] was 0.12 J per pulse. On the other hand, by employing a fixed intensity laser delivering 2 W and running for 2 min, we were able to provide, after careful focusing, a much larger energy of about 200 J/mm^2 per run. As the protocols are slightly different, we shall describe the case of alkali atoms first and then consider the case of nickel.

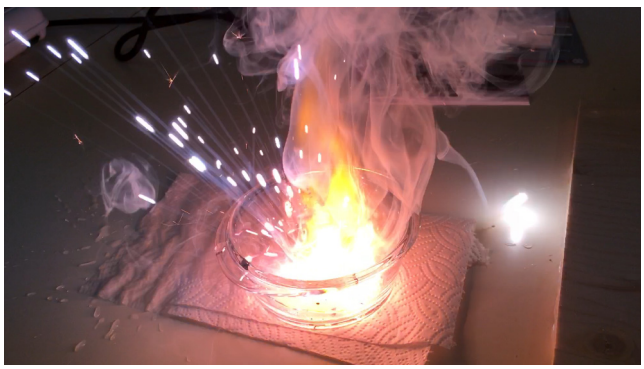

Fig. 9. When cool water was thrown over the melted grains of lithium within a glass bowl, a lithium explosion took place that lasted approximately three seconds. The photograph shown is from a video shot at a frame rate of 240 Hz. The white hot lithium plasma is at the bottom of the explosion and pieces of plasma are blown out as coulomb explosion white hot fragments. The orange fire on top forms lithium oxide and/or hydride colloidal particles which then go up in smoke.

As focused laser light was shone on a few mm^3 pieces of one of the alkali metals, they slowly melted and as they kept absorbing more and more energy, they finally exploded, *without any addition of water*. Some pictures of these explosions can be found at the link provided below in Section (VII). They are a miniature version of the lithium explosions described above in Section 4.1.

On the other hand, for nickel nano-powders, we found it expedient to add water before subjecting them to laser light. In fact, addition of salt seemed to expedite the explosions further. As one can see from the pictures provided in Section (VII), the nickel powder explosion is less virulent than those produced by alkali metals.

4.3. Necessary conditions for LENR in Coulomb explosions

Through Eq. (28), we know that the kinetic energy imparted to an ion is proportional to the cluster radius R. To trigger LENR, in the deuterium beam set up of [15] for example, $R \geqslant 25$ Å. Hence, it is important to be able to determine the "effective" size R of the clusters in a Coulomb explosion.

The cluster size can be measured through light scattering. When the wavelength λ of incident light used for Rayleigh light scattering experiment is large on the scale of the cluster radius R, then the elastic amplitude is determined by the polarizability $\alpha(\omega)$,

$$F_{fi}(\omega) = \left(\frac{\omega}{c}\right)^2 \alpha(\omega)\epsilon_f \cdot \epsilon_i, \tag{33}$$

so the elastic differential cross-section reads

$$\frac{d\sigma}{d\Omega} = |F_{fi}|^2 = \left(\frac{\omega}{c}\right)^4 |\alpha(\omega)|^2 |\epsilon_f \cdot \epsilon_i|^2, \tag{34}$$

and the integrated elastic cross-section reads

$$\sigma_{el} = \left(\frac{8\pi}{3}\right)\left(\frac{\omega}{c}\right)^4 |\alpha(\omega)|^2|. \tag{35}$$

The total cross-section is given by

$$\sigma_{total} = \left(\frac{4\pi c}{\omega}\right)\Im m\ F_{ii} = \left(\frac{4\pi\omega}{c}\right)\Im m\ \alpha(\omega). \tag{36}$$

The radii R of the clusters have been empirically determined previously [15] via light scattering cross-sections as a function of the temperature T of the gas jet producing the clusters. For example, in [15], it was found that at a gas pressure of 55 atmospheres, as the temperature increased from 85 K to 120 K, the measured radii of the clusters decreased from about 55 Å to about 12 Å.

The temperature T of the gas jet producing the clusters also determines the absorption cross-section of the light. Thus, the cluster radius can be determined by the absorption of light. Such measurements have also been made. In addition, the yield as a function of the cluster radius has also been measured. Theoretical estimates are consistent with the experimental results [15].

Of course, for the type of Coulomb explosions discussed in the present paper, the above method has to be suitably modified. We shall discuss the development of such procedures in future work.

5. Conclusions

We have demonstrated several simple experiments which probe low energy collective nuclear chemistry as distinguished from the more usual chemistry based entirely upon electronic structure. The physics of LENR discussed here is through the notion of shredding solids into powders yielding colloidal fluids in either liquid electrolyte and/or gaseous form. These provide benchmark pointers to the large electric fields generated locally. On the other hand, the evidence of low energy nuclear particle production in mechanical engineering labs [13,14] by fractured rocks as well as in geophysical phenomena such as earthquakes, lightning and thunderstorms [9–12] is well documented. We have shown that the acceleration of electrons and ions in both cases of fracturing rocks and electrodes can be comparable. Hence, for the problem at hand, in electrolytic cells, namely batteries, shredding electrodes may also produce low energy nuclear reactions. We have substantiated some nuclear transmutations associated with confined plasmas near the tip of metallic cathodes. We have also shown, starting from a deionized water electrolyte, that a variety of nuclear transmutations can be induced without a plasma so long as the very low current batteries are run for a sufficiently long time. The colloids from shredding cathodes do still appear. Lastly, it was shown that melted liquid lithium in contact with room temperature water gives rise to a bright white hot balled lightning plasma explosion that is simply related to routinely observed lithium ion battery explosions of recent great industrial interest. It is likely that such lithium plasmas have a nuclear component as do many other similar lightning plasmas. Experimental verification of the required conditions and the chemical analysis of the lithium explosion products is presently under study and development.

Supplementary scientific information

Supplementary scientific information such as videos of some of our experiments; pictures of electrolytic cell set ups; further SEM & EDX data on electrodes; Coulomb explosion of alkali metals and nickel nano-powders, can be found at the links [32].

Acknowledgements

The authors thank Dr. M.M. Dadras and Ms. S. Biselli for performing chemical analyses of our samples at CSEM, Jaquet-Droz 1, CH-2002 Neuchâtel CH. YS would like to thank the Department of Physics and Geology at the University of Perugia, Italy, for their hospitality and for providing office space for YS.

Authors AW, YS and LR have received research grants from LENR-Cities Suisse Sàrl, Rue Charles Knapp 29, CH-2000 Neuchâtel CH. Author GM is the owner of the company LENR-Cities Suisse Sàrl, Rue Charles Knapp 29, CH-2000 Neuchâtel CH.

Conflict of interest

The authors declare no conflict of interest.

References

[1] Anderson T. Fracture mechanics. Boca Raton (USA): CRC Press; 1995.
[2] Sun C, Jin Z. Fracture mechanics. Oxford (UK): Academic Press; 2012.
[3] Preparata G. Il Nuovo Cimento 1991;104:1289.
[4] Widom A, Larsen L. Euro Phys J 2006;C46:107. Available from: arXiv:cond-mat/0505026.
[5] Srivastava YN, Widom A, Larsen L. Pramana - J Phys 2010;75:617.
[6] Widom A, Swain J, Srivastava Y. J Phys G Nucl Part Phys 2013;40:015006. Available from: arXiv:1109.4911v2 [phys. gen-ph].
[7] Srivastava YN et al. Key Eng Mater 2013;543:68.
[8] Widom A, Swain J, Srivastava YN. Meccanica 2015;50:1205. Available from: arXiv:1306.6286 [phys. gen-ph].
[9] Plastino W et al. J Radioanal Nucl Chem 2009;282:809.
[10] Plastino W et al. J Environ Radioact 2010;101:45.
[11] Shah G, Razdan H, Bhat C, Ali Q. Nature 1985;313:773.
[12] Gurevich A et al. Phys Rev Lett 2012;108:125001.
[13] Carpinteri A, Lacidogna G, Manuello Amedeo, editors. Acoustic, electromagnetic, neutron emissions from fracture and earthquakes. Berlin: Springer; 2015.
[14] Carpinteri A, Borla O. Eng Fract Mech 2017;177:230.
[15] Zweiback J, Smith R, Cowan T, Hays G, Wharton K, Yanovsky V, et al. Phys Rev Lett 2000;84:2634.
[16] Zweiback J, Smith R, Hartley J, Howell R, Steinke C, Hays G, et al. Phys Rev Lett 2000;85:3640.
[17] Buersgens F, Madison K, Symes D, Hartke R, Osterhoff J, Grigsby W, et al. Phys Rev 2006;E74:016403.
[18] Esry BD et al. Phys Rev Lett 2006;97:013003.
[19] Wu C et al. Phys Chem Chem Phys 2011;13(41):18398.
[20] Leg'are F et al. Phys Rev 2005;A71:013415.
[21] Dash J, Zhu M, Solomon J. Scanning electron microscope and energy dispersive spectrometer studies of metal surfaces before and after interaction with hydrogen isotopes. MIT Colloquium given by John Dash on March 22; 2014.
[22] Mizuno T, Ohmori T, Akimoto T, Takahashi A. Jpn J Appl Phys 2000;39:6055.
[23] Mizuno T, Akimoto T, Ohmori T, Takahashi A. Jpn J Appl Phys 2001;40:L989.
[24] Mizuno T, Akimoto T, Ohmori T, Enyo M. Int J Soc Mat Eng Resour 1998;6:45.
[25] Mizuno T, Ohmori T, Enyo M. Electrochemistry 1996;64:1160.
[26] Cirillo D et al. Key Eng Mater 2012;495:104;
Cirillo D et al. Key Eng Mater 2012;495:124.
[27] Vogt E. TRIUMF Publication no TRI-PP-02-03. Canada: Vancouver; 2002.
[28] The absorption of photons by nuclei (along with the production of neutrons and the subsequent breakup of nuclei) is much enhanced by the phenomenon of giant dipole resonances (GDR). GDR were first discovered experimentally by G.C.Baldwin and G.S. Klaiber, Phys. Rev., 71 (1947) 3 and were theoretically interpreted by M. Goldhaber and E. Teller, Phys. Rev., 74 (1948) 1046 as a collective oscillation of neutrons against protons. It can be understood through an analogy with electric dipoles, where the role of the positive charge is played by the proton and that of the negative charge by neutrons. A compendium of GDR experimental data that are available for all nuclei can be found in [34].
[29] Landau L, Lifshitz E. Electrodynamics of continuous media. Oxford: Pergamon Press; 1984.
[30] Landau L, Lifshitz E. Theory of elasticity, (Section 31). Oxford: Pergamon Press; 1970.
[31] Griffith A. Proc Royal Soc 1921;221:161.
[32] Some pictures and videos of the experiments discussed in the paper can be found at the following links: <http://www.lenr-cities.ch/Article>.
[33] Prialnik D. Stellar structure and evolution, Sec. 4.3. Cambridge: Cambridge University Press; 2000.
[34] Atlas of giant dipole resonances, parameters and graphs of photonuclear reaction cross-sections, A. Varlamov, V. Varlamov, D. Rudenko and M. Stepanov, INDC(NDS)-394, International Atomic Energy Agency, Vienna, Austria (1999).
[35] Details about filtering (sophisticated techniques routinely employed in SEM, EDX devices for finer analyses of signals) can be found in <http://www.charfac.umn.edu/instruments/eds-on-sem-primer.pdf>. <http://cfamm.ucr.edu/documents/eds-intro.pdf>.
[36] Mason PE et al. Nat Chem 2015;2161:1.
[37] Mason PE et al. Angew Chem Int Ed 2016;2016:13019.